PREDICTION OF HYDRODYNAMIC PERFORMANCE OF 3-D WIG BY IBEM

(DOI No: 10.3940/rina.ijme.2018.a3.475)

S Bal, Istanbul Technical University, Turkey

SUMMARY

The hydrodynamic performance of three-dimensional WIG (Wing-In-Ground) vehicle moving with a constant speed above free water surface has been predicted by an Iterative Boundary Element Method (IBEM). IBEM originally developed for 3-D hydrofoils moving under free surface has been modified and extended to 3-D WIGs moving above free water surface. The integral equation based on Green's theorem can be divided into two parts: (1) the wing part, (2) free surface part. These two problems are solved separately, with the effects of one on the other being accounted for in an iterative manner. Both the wing part including the wake surface and the free surface part have been modelled with constant strength dipole and source panels. The effects of Froude number, the height of the hydrofoil from free surface, the sweep, dihedral and anhedral angles on the lift and drag coefficients are discussed for swept and V-type WIGs.

NOMENCLATURE

A	: Planform area (m^2)
c	: Average chord of wing (m)
C_{TIP}	: Chord at tip (m)
C_{ROOT}	: Chord at root (m)
C_D	: Drag coefficient of wing
C_L	: Lift coefficient of wing
C_P	: Pressure coefficient
D	: Drag of wing (N)
Fn	: Chord based Froude number
g	: Gravitational acceleration (m s^{-2})
h	: Clearance between wing and free surface (m)
IBEM	: Iterative boundary element method
k_0	: Wave number (m^{-1})
L	: Lift of wing (N)
$\vec{n}$	: Unit normal vector directed from wing surface to water
P	: Pressure on WIG (Pa)
P_0	: Pressure of incoming flow (Pa)
s	: Span of wing (m)
S_{FS}	: Free surface
S_H	: Wing surface
S_W	: Wake surface
$\vec{t}$	: Unit vector on wake surface
U	: Velocity of incoming flow (m s^{-1})
WIG	: Wing-in-ground
α	: Angle of attack (°)
β	: Dihedral or anhedral angle (°)
Λ	: Sweep angle (°)
Φ	: Total potential (m^2 s)
ϕ	: Perturbation potential (m^2 s)
ρ	: Density of water (kg m^{-3})
ζ	: Wave elevation (m)

1. INTRODUCTION

Marine vehicles operating above the free water surface can utilize wings in order to reach high speeds. WIG (wing-in-ground) effect craft and some racing boats with hydrofoils can take advantage of air lifting surfaces to support completely or partially the vehicle weight. With the help of wings, air can be compressed under the vehicle and an air cushion can be created above the free water surface. This air cushion helps to reduce the drag of the vehicle and only air induced drag occur though the spray formation from water (if exists significantly) can cause an increase in drag. Spray formation can be generated even for surface piercing vehicles and can cause a significant increase in drag. Also an accurate distance between WIG and the free surface may lead to an additional lift force which means additional payload, operating range or speed. Many WIG designs have been made in recent years. Detailed information about design principles of WIG crafts can be found in Rozhdestvensky (2006) and Rozhdestvensky (2010).

A numerical investigation of a wing in ground effect with endplates has been made by taking the free surface deformations into account in Barber (2007). The numerical analyses have been performed for 2-D (two-dimensional) and 3-D (three-dimensional) cases with and without endplates. The numerical results have shown that the deformation on the free surface is caused by wing tip vortices rather than the pressure distribution under the wing. As the Froude number is increased, a small change in the shape of the deformation is observed. At a Froude number of 14 the surface is not a depression, but rather a rise beneath the foil. It was mentioned that this result also followed the trends shown in Grundy (1986). It has also been shown that the endplates in the wing tips have dramatically reduced the free surface deformation. Llifting surface theory has been used in order to solve the flow around a 3-D wing for the inviscid model in Liang and Zong (2011). Ground effect and free surface are taken into account and the wing has been represented by horseshoe vortices using finite number panels. Numerical results have been compared with the experimental ones and the effects of ground clearance on the lift force have been shown for different Mach numbers. In a similar study in Zong and Liang (2012), Prandtl's lifting line theory has been used to calculate the lift force of a wing in the case of ground effect and in the vicinity of a free surface. Linearized free surface boundary condition has been employed using horseshoe vortices for the representation of the wing. The numerical results have

been compared with the experimental data. Matveev (2013) has described a coupled aero-hydrodynamic model for a ram wing moving above water in steady motion. The factors affecting the aerodynamic performance of a ram wing and associated water surface deformations have been presented and it has been shown that an extent of blockage of wing sides can drastically change the ram wing lifting performance. In another study, the span-dominated effect on a wing in close ground proximity has been explained in Abramowski (2007). Moore *et al*. (2002) studied the ground effect of two airfoils experimentally and gave some useful results on the subject. The control of WIG vehicle was also studied in other studies such as; Nebylov and Nebylov (2013), Nebylov and Wilson (2002) and Nebylov (2010). These studies have a large amount of data on the ground effect and control of WIG.

In addition, various numerical methods have been developed to treat the cavitating or non-cavitating flows around hydrofoils moving under free surface. Important studies by using the boundary element methods for the flow analysis of 2-D and 3-D cavitating or non-cavitating hydrofoils and propellers can be found in Fine and Kinnas (1993) and Kinnas and Hsin (1992). Specifically, the Boundary Element Methods (BEMs) have also been found to be computationally efficient and robust tools for the inviscid analysis of cavitating or non-cavitating flows around arbitrary geometries (including ship type of bodies) both in two- and three-dimensions, including the effects of free surface Lee *et al*. (1992). For instance, Rankine types of singularities have modeled the flow around cavitating or non-cavitating hydrofoil under a free surface in Bal *et al*. (2001) and Bal and Kinnas (2002). The linearized free surface condition was used in both methods. An IBEM (iterative boundary element method) for the solution of cavitating or non-cavitating hydrofoils moving under a free surface was described in detail in Bal (2007). The integral equation obtained by applying Green's theorem on the surfaces of the problem was divided into two parts; the hydrofoil part and the free surface part. The hydrofoil influence on the free surface and vice versa were considered via their potential values. Details of the present low-order potential-based panel method can be found in Brebbia *et al*. (1984). One of the most important reviews of boundary element methods up to the late 1970s was given in Cheng and Cheng (2005). In the present study, both the wing surface and the free surface are also modelled with constant strength dipole and constant strength source panels. The source strengths on the free surface are expressed by using linearized free surface condition, in terms of the second derivative of perturbation potential with respect to the horizontal axis. The corresponding second-order derivative is calculated by applying the Dawson's fourth-order backward finite difference scheme Dawson (1977). This iterative method was then modified and extended to apply to the surface piercing bodies inside a numerical towing tank or without a numerical towing tank, the method has been validated with those of others and experiments and extensive numerical results of the method have been presented in Bal (2008) and Bal (2011). In another study, an iterative numerical method has been applied to swept and V-type cavitating hydrofoils moving under free surface and some useful figures for engineers and designers have been given in Bal (2005).

In this study, the performance of a trapezoid WIG wing without endplates moving with a constant speed above free surface has been investigated by an Iterative Boundary Element Method (IBEM). The IBEM has then been applied to swept and V-type (including inverted V-type) WIGs that have been generated from trapezoid WIG and some useful figures for engineers and designers are given. The 3-D WIG geometries in unbounded flow domain have also been investigated with present IBEM. The effects of Froude number, the clearance (height) of the wing from free surface, the dihedral, anhedral and sweep angles on the lift and drag (wave + induced due to lift) coefficients on the aerodynamic performance of the WIG have been discussed.

2. MATHEMATICAL MODEL

It is considered that the WIG above free surface is subjected to a uniform inflow, U. The x-axis is positive in the direction of uniform inflow, the z-axis is positive upwards and the y-axis completes the right-handed system as shown in Figure 1. The wing above undisturbed free surface is located at z = h. It is assumed that the fluid is inviscid and incompressible and the flow field is irrotational. The perturbation potential, ϕ and the total potential, Φ should satisfy the Laplace's equation in the fluid domain,

$$\nabla^2\Phi = \nabla^2\phi = 0 \tag{1}$$

The following boundary conditions should also be satisfied by perturbation potential ϕ:

Kinematic boundary condition: The flow should be tangent to the wing surface,

$$\frac{\partial\phi}{\partial n} = -\vec{U}\cdot\vec{n} \tag{2}$$

where $\vec{n}$ is the unit normal vector to the wing surface directed into the fluid domain.

Kutta condition: The velocity at the trailing edge of the wing should be finite,

$$\nabla\phi = \text{finite; at the trailing edge} \tag{3}$$

An iterative pressure Kutta condition is forced at the trailing edge of the wing, Kinnas and Hsin (1992).

Linearized free surface condition: The following linearized free surface equation should be satisfied:

$$\frac{\partial^2\phi}{\partial x^2}+k_0\frac{\partial\phi}{\partial z}=0 \text{ on } z=0 \tag{4}$$

Here, $k_0=g/U^2$ is the wave number. The corresponding wave elevation in linearized form is as follows:

$$\zeta=-\frac{U}{g}\frac{\partial\phi}{\partial x} \tag{5}$$

Radiation condition: No upstream waves should occur. In order to prevent upstream waves, both the first-derivative and the second-derivative of the perturbation potential with respect to x is forced to be equal to zero for the upstream region on the free surface Bal (2008),

$$\frac{\partial^2\phi}{\partial x^2}=\frac{\partial\phi}{\partial x}=0 \quad \text{as} \quad x\to-\infty \tag{6}$$

3. IBEM

According to the Green's third identity the perturbation potential on the wing surface surface) and on the free surface can be expressed as,

$$2\pi\phi=\int_{S_H+S_{FS}}\left(\phi\frac{\partial G}{\partial n}-\frac{\partial\phi}{\partial n}G\right)dS+\int_{S_W}\Delta\phi_W\frac{\partial G}{\partial n^+}dS \tag{7}$$

where S_H, S_W and S_{FS} are the boundaries of the wing surface, wake surface and the free surface, respectively.

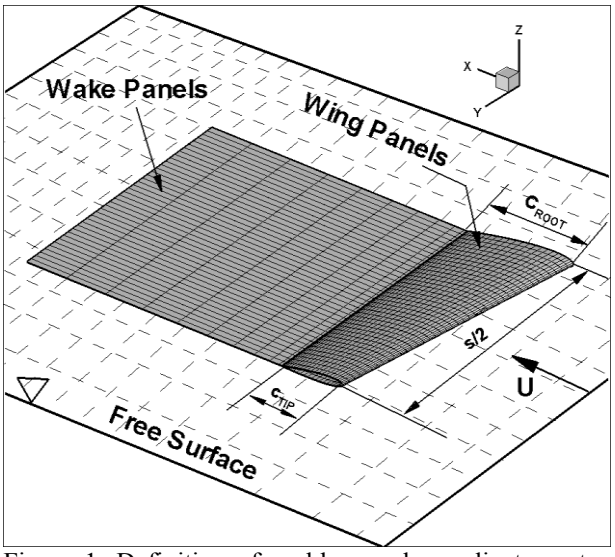

Figure 1: Definition of problem and coordinate system for WIG (Half of the WIG and its wake are shown due to symmetry).

G is the Green function (G=1/r), (r is the distance between the singularity point and field point). $\Delta\phi_W$ is the potential jump across the wake surfaces, and n^+ is the unit vector normal to the wake surface pointing upwards. The iterative method described in Bal (2011) is applied to solve Eq. (7). The iterative method here in general is composed of two parts: (1) the wing part and (2) the free surface part. On the other hand, the potential in the fluid domain due to the influence of the wing, ϕ_H, can be given as,

$$2\pi\phi_H=\int_{S_H}\left(\phi\frac{\partial G}{\partial n}-\frac{\partial\phi}{\partial n}G\right)dS+\int_{S_W}\Delta\phi_W\frac{\partial G}{\partial n^+}dS \tag{8}$$

The potential in the fluid domain due to the influence of the free surface, ϕ_{FS} however, can be given as,

$$2\pi\phi_{FS}=\int_{S_{FS}}\left(\phi\frac{\partial G}{\partial n}-\frac{\partial\phi}{\partial}G\right)dS \tag{9}$$

By substituting Eq. (9) into Eq. (7) and applying the kinematic condition on the wing surface , the following integral equation for the flow on the wing surface can be written as,

$$2\pi\phi=\int_{S_H}\left(\phi\frac{\partial G}{\partial n}+Un_x G\right)dS+\int_{S_W}\Delta\phi_W\frac{\partial G}{\partial n^+}dS+4\pi\phi_{FS} \tag{10}$$

and by substituting Eq. (8) into Eq. (7) similarly and applying the linearized free surface condition, the following integral equation for the flow on the free surface can be written as,

$$2\pi\phi=\int_{S_{FS}}\left(\phi\frac{\partial G}{\partial n}+\frac{\partial^2\phi}{\partial x^2}\frac{G}{k_0}\right)dS+4\pi\phi_H \tag{11}$$

Here, n_x is the x component of normal vector on the wing surface. Integral Equations (10) and (11) can be solved iteratively by a low-order panel method with the potentials ϕ_H and ϕ_{FS} being updated during the iterative process. Here, the wing surface and the free surface communicate each other via potential. The wing surface and the free surface are discretized into panels with constant strength source and dipole distributions. The discretized integral equations provide two matrix equations with respect to the unknown potential values and can be solved by any matrix solver. In Eq.(20), the second derivative of perturbation potential term $(\partial^2\phi/\partial x^2)$ can be expressed in terms of the potentials on the free surface by applying Dawson's original fourth-order backward finite difference scheme as given in Bal *et al*. (2001). In order to prevent upstream waves, the first derivative of potential with respect to x, $(\partial\phi/\partial x)$ (which corresponds to the wave deformation) and the second derivative of potential with respect to x, $(\partial^2\phi/\partial x^2)$ (which corresponds to first derivative of wave deformation) are enforced to be equal to zero Bal and

Kinnas (2002). Thus the source strengths from some distance (termed *radiation distance*) in front of the hydrofoil to the upstream truncation boundary of the free surface are set to zero, and this forces the first derivative of potential with respect to z ($\partial\phi/\partial z$) to be equal to zero. The value of radiation distance is kept the same along the y axis. Details of the numerical method can be found in Bal (2011).

4. NUMERICAL RESULTS

The method (IBEM) was validated before with the results of other numerical methods and experiments for different cases in the literature (Bal and Kinnas (2002), Bal (2011), Bal (2016), Kinaci and Bal (2016), Dogrul and Bal (2016)). Here, the method is first applied to the case of trapezoid 3-D WIG which has NACA0012 sections along span-wise direction. The ratio of chord length at the tip to span of the wing and the ratio of chord length at the root to span of the wing are represented as $C_{TIP}/S=0.06065$, $C_{ROOT}/S=0.10435$, respectively, as shown in Figure 1.

The average chord length is defined as $c=0.5*(C_{TIP}+C_{ROOT})$. The analyses have been performed for the angle of attack, $\alpha=5°$. The total number of panels on the wing is 50x40x2=8000, (the number of panels along chord-wise direction and span-wise direction are 50 and 40, respectively) as shown half of the wing due to symmetry with respect to span in Figure 1. On the other hand the total number of panels on the free surface is selected as 100x20=2000, (the number of panels along x direction and y direction are 100 and 20, respectively). In Figure 2, the variation of lift and drag coefficients (induced drag + wave drag) coefficients;

$$\left(C_L=\frac{L}{\frac{1}{2}\rho AU^2}, C_D=\frac{D}{\frac{1}{2}\rho AU^2},\right.$$

L: lift force,
D: drag force,
A: planform area of the wing) with Froude number $\left(Fn=\frac{U}{\sqrt{gc}}\right)$ is presented for two different h/c ratios (=0.75 and 1.50).

The lift and drag coefficients (only induced) in the case of unbounded (infinite) flow domain (no free surface effect) are computed as $C_L=0.2611$ and $C_D=0.0060$, respectively. Therefore for the Froude numbers up to Fn=0.9, the free surface caused an increase in lift coefficients and for the whole range of Froude numbers, it caused a decrease in drag coefficients as compared with those of unbounded flow domain.

In Figure 3, the effect of Froude number on non-dimensional pressure coefficients $\left(C_p=\frac{p_0-p}{\frac{1}{2}\rho U^2}\right)$ on the pressure side of WIG have been shown as compared with those of infinite case (no free surface, unbounded flow domain) solution. The non-dimensional pressure distribution on the mid-strip (root chord) for Fn=0.7 and h/c=0.75 are also given as compared with those of unbounded flow domain solution in Figure 4. The free surface affected the pressure side of the WIG larger than the suction side, as expected. It means that the free surface causes higher loading (lift coefficient) on the WIG for this case that is consistent with the lift coefficient given in Figure 2.

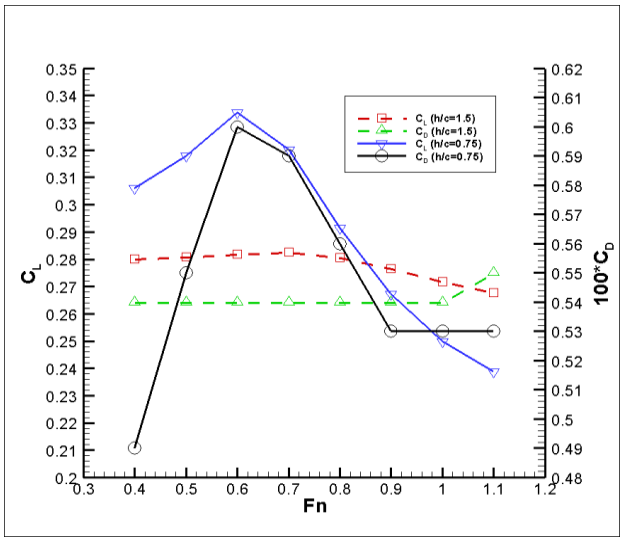

Figure 2: Variation of lift and drag coefficients with Froude number and clearance from free surface at angle of attack $\alpha=5°$.

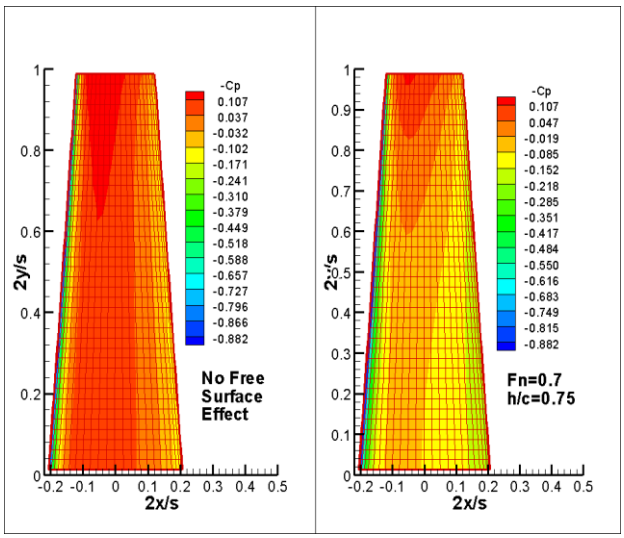

Figure 3: Non-dimensional pressure contours on suction (upper) side of both wings (no free surface effect).

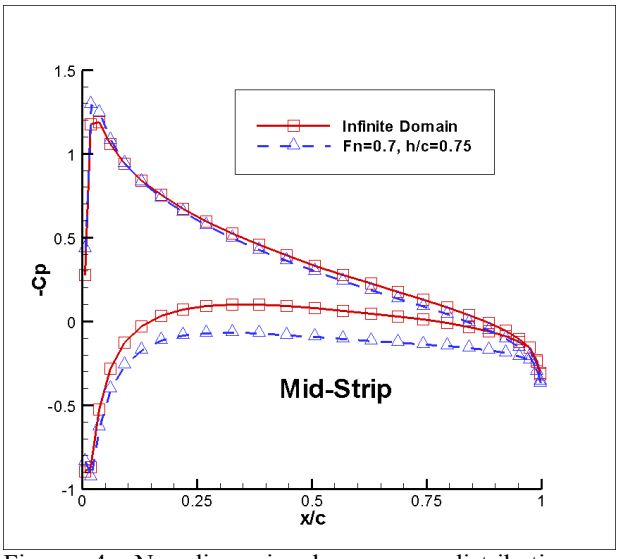

Figure 4: Non-dimensional pressure distribution on rectangular wing with AR=4.

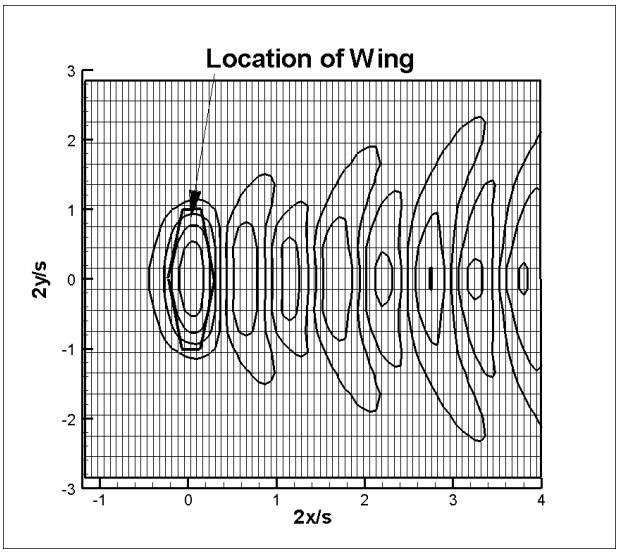

Figure 5: Kelvin wave contours on free surface.

In Figure 5, the wave contours on the free surface by IBEM are shown for Fn=0.7 and h/c=0.75. The Kelvin wave pattern can be seen clearly here.

The method has later been applied to V-type and inverted V-type WIGs. It is assumed that the dihedral angle of V-type WIG is β=11.3° and the anhedral angle of inverted V-type WIG is β=-11.3°. In Figure 6, the definitions of dihedral and anhedral angles are shown with the panels used in the calculations. The WIGs have NACA0012 sections along their span-wise direction. Angle of attack is chosen as α=5° degrees. The case of β=0° corresponds to the trapezoid WIG. The ratio of clearance between WIG and free surface to average chord length is h/c=0.75. Effect of dihedral and anhedral angles on lift and drag coefficients are shown in Figures 7 and 8, respectively. The lift and drag coefficients (only induced) in the case of unbounded (infinite) flow domain (no free surface effect) are computed as C_L=0.2623 and C_D=0.0059 for V-type wing and C_L=0.2547 and C_D=0.0057 for inverted V-type wing, respectively. Therefore for the Froude numbers up to Fn=0.8, V-type WIG has larger lift values and on the other hand for bigger Froude numbers than 0.8, inverted V-type WIG generates larger lift coefficients. The same is true for drag coefficients as well.

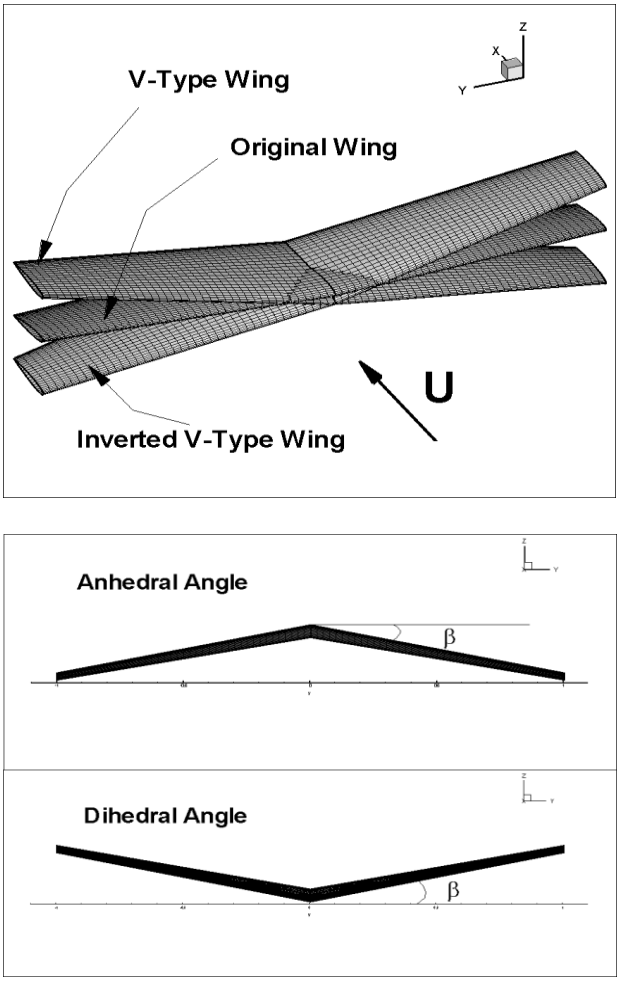

Figure 6: Definition of anhedral, dihedral angles and V-type, inverted V-type wings.

Lastly, the method (IBEM) has been applied to swept-type WIGs. The sweep angles of first and second swept WIGs are chosen as Λ=15.9° and 26.1°, respectively. In Figure 9, the definition of swept angle is shown with the panels used in the calculations. The WIGs have NACA0012 sections along their span-wise direction. Angle of attack is chosen as α=5° degrees. The case of Λ=0° corresponds to the trapezoid WIG. The ratio of clearance between WIG and free surface to average chord length is h/c=0.75. Effect of sweep angles on lift and drag coefficients are shown in Figures 10 and 11, respectively. The lift and drag coefficients (only induced) in the case of unbounded (infinite) flow domain (no free surface effect) are computed as C_L=0.2597 and C_D=0.0059 for swept wing 1 and C_L=0.2533 and

C_D=0.0056 for swept wing 2, respectively. For the selected range of Froude numbers, original WIG generates larger lift values.

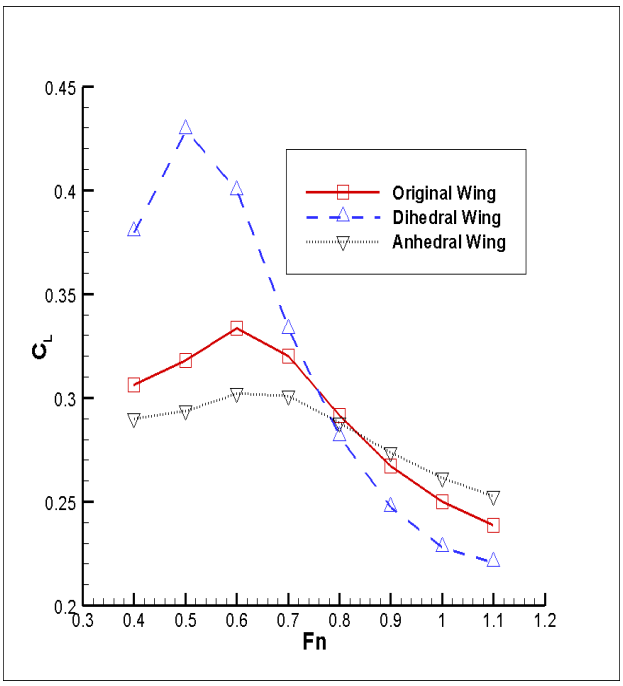

Figure 7: Variation of lift coefficients with Froude number for h/c=0.75 at angle of attack α=5°.

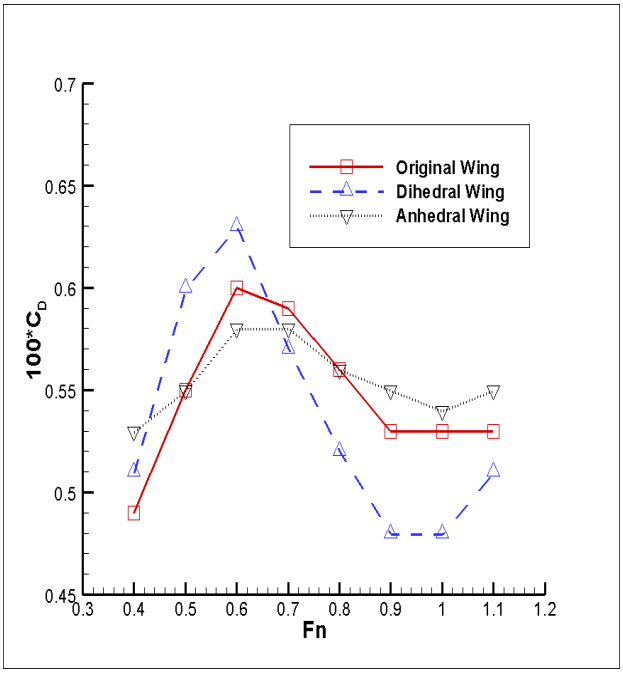

Figure 8: Variation of drag coefficients with Froude number for h/c=0.75 at angle of attack α=5°.

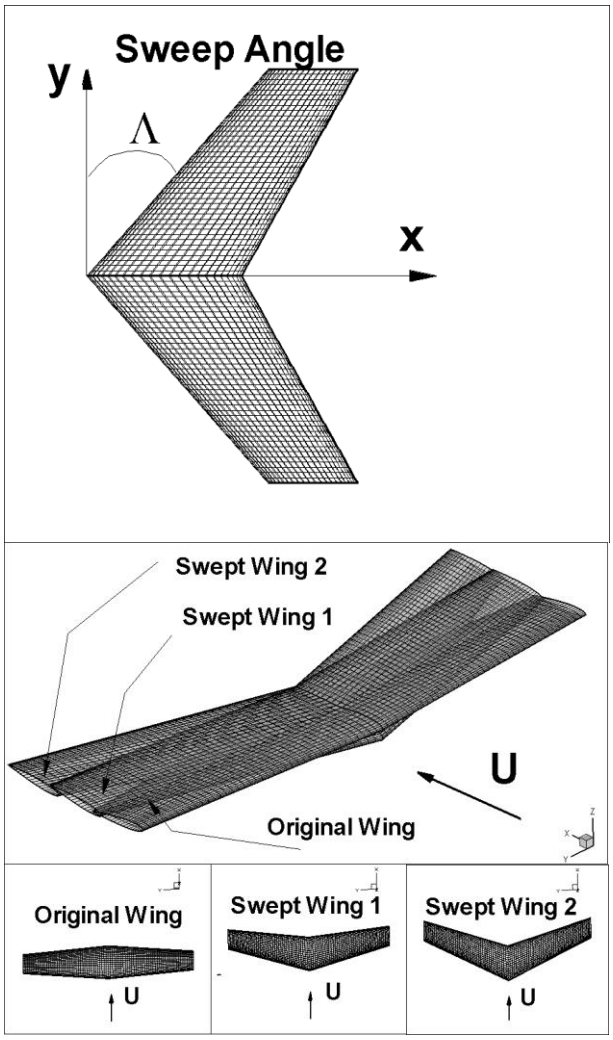

Figure 9: Definition of sweep angle and swept-type wings.

5. CONCLUSIONS

In the present paper, an IBEM (terative boundary element method) developed originally before for cavitating hydrofoils moving under free surface has been modified and extended to predict the aerodynamic performance of 3-D WIG moving steadily over a free water surface. The IBEM has then been applied to swept and V-type, including inverted V-type WIGs and some useful figures for engineers and designers are given. All generated 3-D WIG geometries in unbounded flow domain have also been investigated with present IBEM. The followings have been found:

1. All parameters of the problem such as dihedral, anhedral and swept angles, Froude number and clearance (height) between WIG and free surface are substantial and should be considered in the design stage of the WIGs.
2. If the clearance is small, free surface effect on WIG becomes significant for a large range of Froude numbers.

3. The Kelvin wave pattern has also been occurred on the free water surface for the selected range of Froude numbers.
4. While V-type WIG has larger lift values for certain range of Froude numbers (0.4<Fn<0.8), the inverted V-type WIG generates larger lift coefficients for Froude numbers bigger than 0.8 (Fn>0.8). The same is true for drag coefficients as well.
5. Sweep angles on the other hand has caused a decrease in lift coefficient for selected range of Froude numbers.

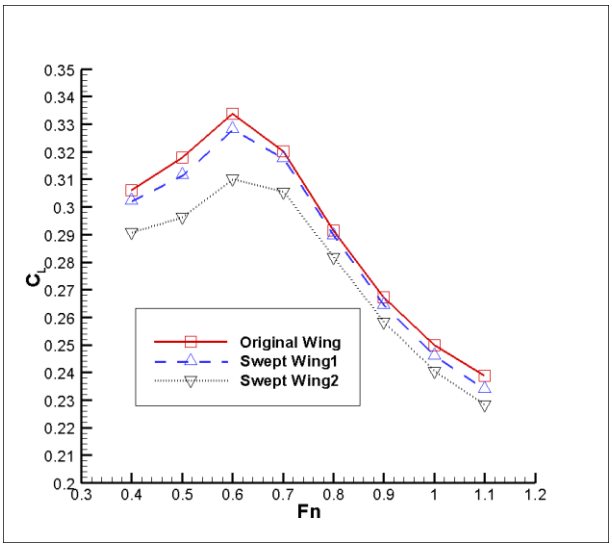

Figure 10: Variation of lift coefficients with Froude number for h/c=0.75 at angle of attack α=5°.

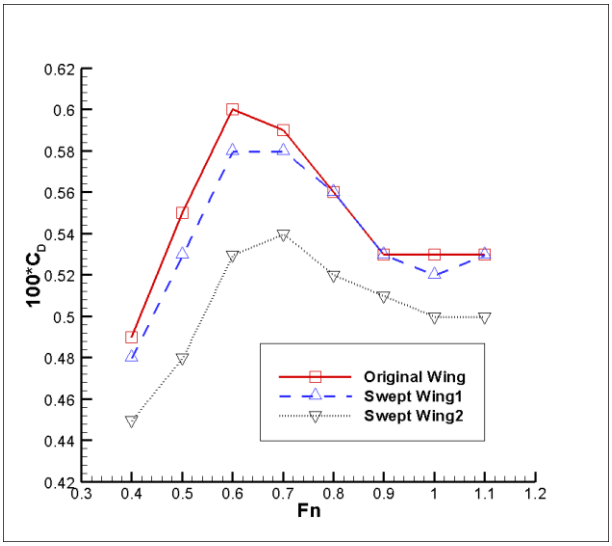

Figure 11: Variation of drag coefficients with Froude number for h/c=0.75 at angle of attack α=5°.

6. REFERENCES

1. ABRAMOWSKI, T. (2007). "Numerical investigation of airfoil in ground proximity", *Journal of Theoretical and Applied Mechanics*, 45, 2, pp 425-436.
2. BAL, S (2005). "Lift and drag characteristics of cavitating wwept and V-type hydrofoils", *Trans of RINA, International Journal of Maritime Engineering*, 147, Part A, pp 51-64.
3. BAL, S (2007). "A numerical method for the prediction of wave pattern of surface piercing cavitating hydrofoils", *Proceedings of the Institution of Mechanical Engineers, Part C, Journal of Mechanical Engineering Sciences*, 221, pp 1623-1633.
4. BAL, S (2008). "Performance prediction of surface piercing bodies in numerical towing tank", *International Journal of Offshore and Polar Engineering*, 18, pp 106-111.
5. BAL, S (2011). "The effect of finite depth on 2-D and 3-D cavitating hydrofoils", *Journal of Marine Science and Technology*, 16, 2, pp 129-142.
6. BAL, S (2016). "Free surface effects on 2-D airfoils and 3-D wings moving over water", *Ocean Systems Engineering, An International Journal*, 6, 3, pp 245-264.
7. BAL, S. and KINNAS, SA (2002). "A BEM for the prediction of free surface effect on cavitating hydrofoils", *Computational Mechanics*, 28, pp 260-274.
8. BAL, S., KINNAS SA and LEE, H (2001). "Numerical analysis of 2-D and 3-D cavitating hydrofoils under a free surface", *Journal of Ship Research*, 45, 1, pp 34-49.
9. BARBER, TJ (2007). "A study of water surface deformation due to tip vortices of a wing-in-ground effect", *Journal of Ship Research*, 51, 2, pp 182–186.
10. BREBBIA, CA, TELLES, JCF and WROBEL, LC (1984). "*Boundary element techniques-theory and applications in engineering"*, Springer-Verlag, Berlin, Germany.
11. CHENG, AHD and CHENG, DT (2005). "Heritage and early history of the boundary element method", *Engineering Analysis with Boundary Elements*, 29, pp 268-302.
12. DAWSON, DW (1977). "A practical computer method for solving ship-wave problems", *2nd International Conference on Numerical Ship Hydrodynamics*, USA.
13. DOGRUL, A and BAL, S (2016). "Performance prediction of wings moving above free surface", *Advances in Boundary Element and Meshless Techniques XVII*, pp 85-92, Middle East Technical University, Ankara, Turkey, July 11-13.
14. FINE, NE and KINNAS, SA (1993). "A boundary element method for the analysis of the

flow around 3-D cavitating hydrofoils", *Journal of Ship Research*, 37, pp 213-224.

15. GRUNDY, I (1986). "Airfoils moving in air close to a dynamic water surface", *Journal of the Australian Mathematical Society Series B*, 27, 3, pp 327—345.
16. KINACI, OK and BAL, S (2016). "Performance prediction of 2D foils moving above and close to free surface", *Advances in Boundary Element and Meshless Techniques XVII*, pp: 43-50, Middle East Technical University, Ankara, Turkey, July 11-13.
17. KINNAS, SA and HSIN, CY (1992). "A boundary element method for the analysis of the unsteady flow around extreme propeller geometries", *AIAA Journal*, 30, pp 688-696.
18. LEE, CS, LEW, CW and KIM, YG (1992). "Analysis of a two-dimensional partially or supercavitating hydrofoil advancing under a free surface with a finite Froude number", *19th Symposium on Naval Hydrodynamics*, pp 605-618, Korea.
19. LIANG, H and ZONG, Z (2011). "A subsonic lifting surface theory for wing-in-ground effect", *Acta Mechanica*, 219, 3–4, pp 203–217.
20. MATVEEV, KI (2013). "Modeling of finite-span ram wings moving above water of finite Froude numbers", *Journal of Ship Research*, 58, 3, pp 146-156.
21. MOORE, N, WILSON, PA and PETERS, AJ (2002). "An investigation into wing in ground effect aerofoil geometry", In RTO-MP-095, NATO RTO., 11-[20pp].
22. NEBYLOV, AV (2010). "Principles and systems of heavy WIG-craft flight control", *18th IFAC Symposium on Automatic Control in Aerospace*, Nara, Japan.
23. NEBYLOV, AV and NEBYLOV, VA (2013). "WIG-Craft Flight Control Systems Development", *5th European Conference for Aerospace Sciences (EUCASS)*, Minich, Germany.
24. NEBYLOV, AV and WİLSON, PA (2002). Ekranoplane - Controlled Flight close to Surface. Monograph. WIT-Press, Southampton, UK, 226 pp.
25. ROZHDESTVENSKY, KV (2006). "Wing-in-ground effect vehicles", *Progress in Aerospace Sciences*, 42, 3, pp 211–283.
26. ROZHDESTVENSKY, KV (2010). "*Aerodynamics of a lifting system in extreme ground effect*", Springer-Verlag Berlin and Heidelberg GmbH & Co. K, Germany.
27. ZONG, Z, LIANG, H and ZHOU, L (2012). "Lifting line theory for wing-in-ground effect in proximity to a free surface", *Journal of Engineering Mathematics*, 74, 1, pp 143–158.

